Orbits of massless particles in the Schwarzschild metric: Exact solutions

Gerardo Muñoz

ARTICLES YOU MAY BE INTERESTED IN

The Schwarzschild metric: It's the coordinates, stupid!
American Journal of Physics **82**, 295 (2014); https://doi.org/10.1119/1.4850396

Visualizing circular motion around a Schwarzschild black hole
American Journal of Physics **79**, 63 (2011); https://doi.org/10.1119/1.3492722

Wormholes in spacetime and their use for interstellar travel: A tool for teaching general relativity
American Journal of Physics **56**, 395 (1988); https://doi.org/10.1119/1.15620

Space-time geometries characterized by solutions to the geodesic equations
Computers in Physics **6**, 498 (1992); https://doi.org/10.1063/1.168437

Visualizing Interstellar's Wormhole
American Journal of Physics **83**, 486 (2015); https://doi.org/10.1119/1.4916949

Motion of test particles in a regular black hole space–time
Journal of Mathematical Physics **56**, 032501 (2015); https://doi.org/10.1063/1.4913882

Orbits of massless particles in the Schwarzschild metric: Exact solutions

Gerardo Muñoz[a]

Department of Physics, California State University, Fresno, Fresno, California 93740-8031

The problem of finding all the orbits of test particles in the exterior Schwarzschild black hole metric has an exact solution in terms of elliptic functions. In this paper, we develop in detail the case of massless particles, including a derivation of an exact formula for the deflection of light. It is shown that the mass of the black hole can be determined from a simple relationship between the angular deflection and the time delay of neighboring light rays. © *2014 American Association of Physics Teachers.*
[http://dx.doi.org/10.1119/1.4866274]

I. INTRODUCTION

Because of its simplicity as well as its historical importance, the Schwarzschild solution is familiar to anybody who has studied general relativity. Some of its consequences—the precession of perihelia and the deflection of light in particular—helped convince many physicists that Einstein's theory was the correct description of relativistic gravitation.

It is therefore somewhat surprising that a complete classification of the allowed orbits in the Schwarzschild geometry is conspicuously absent from the standard literature on general relativity. This does not mean, of course, that such a classification is impossible or that it has not been carried out. Indeed, already in 1917 a remarkable paper by Droste[1] presented exact solutions for the orbits of massive particles in addition to an independent derivation of the Schwarzschild metric. In 1931, Hagihara[2] published a comprehensive treatment of all trajectories for massive particles based on the Hamilton-Jacobi equation. The massless case was viewed as a limit and relegated to a few comments; in particular, no explicit formulas for the trajectories were presented. Mielnik and Plebański,[3] building on previous work by Darwin[4] and apparently unaware of the papers by Droste or Hagihara, rederived the complete solution for the massive case in 1962. These early efforts culminated in the publication of S. Chandrasekhar's *The Mathematical Theory of Black Holes*,[5] where the solutions for both massive and massless cases were given. More recently, Čadež and Kostić[6] revisited the problem of lightlike geodesics in order to develop ray-tracing optics in the Schwarzschild space-time, and Müller[7] discussed the determination of black hole masses by means of their Einstein rings.

Most of the papers listed above make use of the Weierstrass elliptic function for their final expressions and, with the exceptions of Hagihara and Chandrasekhar, make no attempt to produce visual representations of the rich diversity of trajectories contained in their analytic formulas. Furthermore, perhaps as a natural corollary of their timid attitude toward exact solutions, textbooks rarely venture to treat the deflection of light beyond the weak-field limit of Schwarzschild despite the fact that the most interesting novel features of relativistic gravity are known to emerge in the opposite limit. We believe, however, that exposure to even a minimal qualitative understanding of the complex structure of the strong-field orbits is essential for serious students of general relativity. The purpose of this paper is to provide that exposure by concentrating on a classification of the orbits of photons based on the somewhat simpler Jacobi elliptic functions, with an emphasis on the

visualization of the general answers. We also provide an exact formula for the deflection of light, and a new method to determine the mass of a black hole from angular deflection and time dilation data.

As experimental tests of general relativity move beyond the linear approximation, exact predictions for simple phenomena such as the deflection of light will become essential to the discrimination between alternative theories of gravity and to practical work in astrophysics and cosmology. For this reason, a substantial amount of effort has been devoted in recent years to studying the properties of null geodesics in various geometries, and it is hoped that the present paper will serve a dual purpose as an introduction to the more advanced literature. The interested reader wishing to go beyond the scope of our discussion may find Refs. 5, 8–10, and references therein, useful. Solutions for Reissner-Nordström, Kerr, and Kerr-Newman spacetimes can be found in Chandrasekhar's book;[5] Gibbons and Vyska[8] extended the analysis of null geodesics to other spacetimes and higher dimensions; Hackmann and Lämmerzahl[9] give a complete set of solutions for Schwarzschild anti-de Sitter; and Hackmann, Hartmann, Lämmerzahl, and Sirimachan[10] provide the solutions applicable to a Schwarzschild black hole pierced by a cosmic string.

II. THE EQUATION OF MOTION FOR MASSLESS PARTICLES IN THE SCHWARZSCHILD METRIC

The Schwarzschild metric is[11–16]

$$ds^2 = -\left(1 - \frac{R_S}{r}\right)c^2 dt^2 + \left(1 - \frac{R_S}{r}\right)^{-1} dr^2$$
$$+ r^2\left(d\theta^2 + \sin^2\theta\, d\phi^2\right) \tag{1}$$

with $R_S = 2GM/c^2$ the Schwarzschild radius. As is intuitively clear, the more dramatic deviations from a Newtonian behavior will emerge if the particles are able to get very close to R_S. For this reason, we shall assume that we are dealing with a Schwarzschild black hole and will solve the equations of motion for the exterior region $r > R_S$.

Massless particles follow null geodesics ($ds^2 = 0$) so that the proper time interval along the spacetime path is zero. A convenient way to deal with the lack of a proper time is to regard the trajectory as a function of an arbitrary affine parameter λ and to view the geodesic as defined by the parallel transport of the null tangent vector $k^\mu = dx^\mu/d\lambda$. Written in terms of the covariant components k_μ, this condition reads

$$\frac{dk_\mu}{d\lambda} = \Gamma^\nu_{\mu\sigma} k_\nu k^\sigma. \tag{2}$$

A straightforward computation using the definition of the Christoffel symbols yields the equivalent form

$$\frac{dk_\mu}{d\lambda} = \frac{1}{2} k^\nu k^\sigma \, \partial_\mu g_{\nu\sigma}. \tag{3}$$

Because the metric $g_{\nu\sigma}$ is independent of $x^0 = ct$ as well as $x^3 = \phi$, this form of the geodesic equation makes the conservation of k_0 and k_3 evident (a dot indicates a derivative $d/d\lambda$):

$$k_0 = g_{00} k^0 = -\left(1 - \frac{R_S}{r}\right)\dot{x}^0 = \text{constant}; \tag{4}$$

$$k_3 = g_{33} k^3 = r^2 \sin^2\theta \, \dot{\phi} = \text{constant}. \tag{5}$$

For $\mu = 2$, Eq. (3) can be combined with Eq. (5) to prove that if we orient our coordinate system so that the motion starts in the plane $\theta = \pi/2$ with $\dot{\theta} = 0$, then $\ddot{\theta} = 0$ and the subsequent motion must remain in the equatorial plane. The obvious connection with the restriction coming from angular momentum conservation in Newtonian mechanics can be made explicit by considering the quantity $\boldsymbol{\ell} = \mathbf{r} \times \dot{\mathbf{r}}$, with $\mathbf{r}$ and $\dot{\mathbf{r}} = d\mathbf{r}/d\lambda$ ordinary 3-vectors. The geodesic equation implies that $\dot{\boldsymbol{\ell}} = 0$, and standard arguments can be used to conclude again that the orbit is constrained to a plane. From now on, we shall assume that the coordinate system has been chosen so that $\theta = \pi/2$ specifies that plane (note that this means that $k_2 = 0$).

The meaning of $k_3 = r^2 \dot{\phi}$ as proportional to the photon's angular momentum should be clear. The physical meaning of k_0 is easiest to identify for photons that start out at infinity, since there the fact that this vector is null reads $\eta_{\nu\sigma} k^\nu k^\sigma = 0$, with η the flat spacetime metric, so $k^\mu = -k_0(1, \hat{\mathbf{k}})$. Because the photon's 4-momentum at infinity is $p^\mu = (E/c)(1, \hat{\mathbf{k}})$, we can always adjust the normalization of the affine parameter λ so as to have $k_0 = -E/c$ (i.e., $k^\mu = p^\mu$), and the conservation of k_0 then ensures that this interpretation can be maintained for all later times. An additional advantage of this normalization is that the meaning of k_3 reverts to a more familiar form. From Eq. (4), we have $d\lambda = c^2 dt/E$ as $r \to \infty$; hence

$$k_3 \to \frac{E}{c^2} r^2 \frac{d\phi}{dt} \tag{6}$$

in the same limit. Since $\mathbf{p} = (E/c)\hat{\mathbf{k}} = (E/c^2)\mathbf{v}$, the orbital angular momentum of the photon is $\mathbf{L} = \mathbf{r} \times \mathbf{p} = k_3 \hat{\mathbf{z}}$. As with k_0, conservation of k_3 means that the identification $k_3 = L$ will hold for all times, and we can rewrite Eqs. (4) and (5) as

$$\frac{dx^0}{d\lambda} = \frac{E/c}{1 - R_S/r}; \tag{7}$$

$$\frac{d\phi}{d\lambda} = \frac{L}{r^2}. \tag{8}$$

For photons that do not begin (or end) at infinity, we can simply define λ so that $k_0 = -E/c$ with E the energy of the photon at, say, the point of release, so that with an appropriate interpretation of E and L the above relations can always

be used. Substituting into $ds^2/d\lambda^2 = 0$ and rearranging we find

$$\left(\frac{dr}{d\lambda}\right)^2 + \frac{L^2}{r^2}\left(1 - \frac{R_S}{r}\right) = \left(\frac{E}{c}\right)^2, \tag{9}$$

or, writing $u = R_S/r$ and $u' = du/d\phi$,

$$u'^2 + u^2(1 - u) = \left(\frac{ER_S}{Lc}\right)^2. \tag{10}$$

The combination of parameters on the right-hand side can be viewed as $(R_S/b)^2$, with $b = Lc/E$ the impact parameter, or as $(L_0/L)^2$, with $L_0 = ER_S/c$ a characteristic angular momentum for the system. Equation (10) will be the springboard for our derivation of the possible photon orbits in the following sections. Note that the variable u must lie in the range $0 < u < 1$ for orbits in the exterior region.

III. THE EFFECTIVE POTENTIAL AND QUALITATIVE PROPERTIES OF THE ORBITS

In this section, we briefly review, for completeness, some well-known general properties of the orbits that can be extracted from an analysis of the effective potential.[12–15]

In Eq. (9), we let

$$V_{\text{eff}} = \left(\frac{R_S}{r}\right)^2\left(1 - \frac{R_S}{r}\right). \tag{11}$$

This function has the simple shape shown in Fig. 1: it is always positive for $r > R_S$, tends to zero at infinity, reaches a maximum at $r = 3R_S/2$, at which point $V_{\text{eff}} = (2/3\sqrt{3})^2$, and decreases to zero at $r = R_S$. The photon can reach a turning point only if $dr/d\lambda = 0$, i.e. only if the initial conditions are such that $V_{\text{eff}} = (R_S/b)^2$ for some r. Since the effective potential has a maximum, we see that there are no turning points if $b < b_{\text{crit}} \equiv 3\sqrt{3}R_S/2$. In this situation, illustrated by the top horizontal line in Fig. 1, a photon starting out at infinity would necessarily cross the event horizon and fall into the black hole. A photon directed outward would eventually reach infinity. For $b = b_{\text{crit}}$, the photon can settle at the maximum of V_{eff} and remain in a circular orbit at $r = 3R_S/2$ (not surprisingly, this orbit is unstable). The short horizontal line
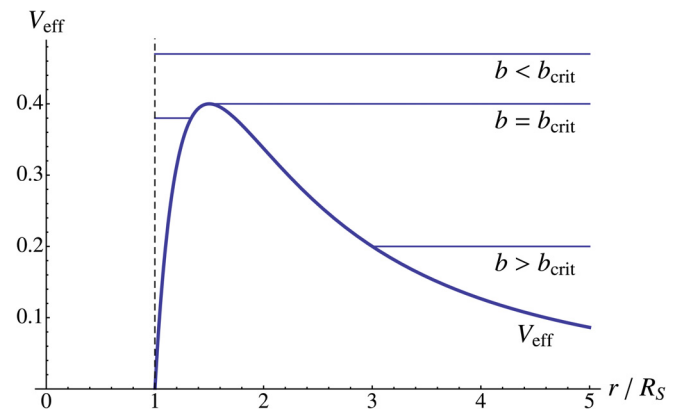
Fig. 1. Effective potential and possible trajectories as a function of the impact parameter b. A trajectory at $b = b_{\text{crit}}$ to the left of the maximum of V_{eff} has been omitted for clarity. The dashed vertical line indicates the position of the event horizon.

to the left of the maximum represents a photon with $b > b_{\text{crit}}$ (the equivalent condition $L > L_{\text{crit}} \equiv 3\sqrt{3}ER_S/2c$ is perhaps more useful here). If this photon is initially directed away from the event horizon, it will reach a turning point and fall into the black hole. If it is directed toward the event horizon it simply falls in. The bottom horizontal line depicts a photon with $b > b_{\text{crit}}$; this photon will reach a minimum value of r and then recede back to infinity.

Although the details of the motion are not revealed by this approach, it is nevertheless valuable because it tells us that the orbits are classified by the value of the impact parameter relative to the critical impact parameter b_{crit} (or equivalently, by the relationship between the angular momentum L and the critical angular momentum L_{crit}). It also shows that there are no stable bound orbits for photons, since V_{eff} has no minima for finite r.

IV. EXACT SOLUTIONS IN TERMS OF JACOBI ELLIPTIC FUNCTIONS

We now seek the explicit form of the solutions outlined in the previous section. Because generic trajectories with $L = 0$ are fairly trivial—see Eq. (9)—we will assume $L \neq 0$ in all the developments below. Our approach closely follows Lawden's[17] method for nonrelativistic central potentials. Lawden gives a very readable, detailed exposition of Jacobi elliptic functions with many examples from physics. In addition, a brief summary and properties of Jacobi elliptic functions in the context of the problem of a bead on a hoop appeared recently in the pages of this journal.[18] Numerous related applications to Newtonian dynamics can be found in Refs. 19 and 20.

As a first step, write Eq. (10) as

$$u'^2 = f(u) \tag{12}$$

with

$$f(u) = \left(\frac{ER_S}{Lc}\right)^2 + u^3 - u^2. \tag{13}$$

We notice immediately from Eq. (12) that $f(u) \geq 0$ and that the solutions of $f(u) = 0$ play an important role in determining the orbits: if $f(u)$ vanishes for some real positive value of u, Eq. (12) indicates that we either have a circular orbit or a turning point in a non-circular orbit. As we shall see, no inflection points arise for photons. The reader is encouraged at this point to repeat the qualitative analysis in Sec. III in terms of $f(u)$.

The roots of $f(u) = 0$ are conveniently given in terms of the quantity

$$\xi = x - \sqrt{x^2 - 1}, \tag{14}$$

where

$$x = \frac{3\sqrt{3}}{2}\frac{ER_S}{Lc} = \frac{b_{\text{crit}}}{b} = \frac{L_{\text{crit}}}{L}, \tag{15}$$

as

$$u_1 = \frac{1}{3}\left(1 - \xi^{2/3} - \xi^{-2/3}\right), \tag{16}$$

$$u_2 = \frac{1}{3}\left(1 + e^{-i\pi/3}\,\xi^{2/3} + e^{i\pi/3}\,\xi^{-2/3}\right), \tag{17}$$

$$u_3 = \frac{1}{3}\left(1 + e^{i\pi/3}\,\xi^{2/3} + e^{-i\pi/3}\,\xi^{-2/3}\right). \tag{18}$$

The right-hand side of Eq. (12) then becomes

$$f(u) = (u - u_1)(u - u_2)(u - u_3), \tag{19}$$

which makes it apparent that the allowed orbits are intimately related to the nature of the roots, since f cannot be negative. For instance, one could in principle imagine a case where $u_1 > u_2 > u_3 > 0$. This would make it possible for u to vary between u_2 and u_3, proving the existence of a non-circular bound photon orbit. To decide whether a case like this is indeed realized (it is not!) and completely characterize the motion, we need to understand the root structure of $f(u)$. The roots are, in turn, controlled by x, i.e., by the relationship between the impact parameter b and the critical impact parameter b_{crit} (equivalently, between L and L_{crit}). Let us therefore examine the different possibilities that arise as we vary x.

A. $x = 1$ ($b = b_{\text{crit}}$; $L = L_{\text{crit}}$)

This case is fairly simple: for $x = 1$, we have $\xi = 1$ and all the roots are real:

$$u_1 = -\frac{1}{3}, \tag{20}$$

$$u_2 = u_3 = \frac{2}{3}. \tag{21}$$

The orbit equation (12) reduces to

$$u'^2 = \left(u + \frac{1}{3}\right)\left(u - \frac{2}{3}\right)^2. \tag{22}$$

Recalling that u is positive by definition, we see that $u' = 0$ is a physical solution only if $u = 2/3$. This is a circular orbit with $r = 3R_S/2$ that sits at the maximum of the effective potential in Fig. 1. Perturbing this solution by substituting $u = 2/3 + \delta u$ into Eq. (22) shows immediately that the circular orbit is unstable.

For $u' \neq 0$, we have two possibilities, $u' = \pm(u - 2/3)$ $\sqrt{u + 1/3}$. The plus (minus) sign indicates outward (inward) motion for $0 < u \leq 2/3$, while the opposite is true for $2/3 \leq u < 1$. These differential equations are not difficult to integrate directly; we find

$$r = \frac{R_S}{\tanh^2[(\phi - \alpha)/2] - 1/3} \tag{23}$$

for $3R_S/2 \leq r < \infty$, and

$$r = \frac{R_S}{\coth^2[(\phi - \alpha)/2)] - 1/3} \tag{24}$$

for $R_S < r \leq 3R_S/2$. In these solutions, α is an integration constant that can be determined by imposing initial conditions. Equation (23) represents an in-spiraling motion when the initial angle $\phi_0 > \alpha$. For instance, we might start with a photon at infinity; choosing $\phi_0 = 0$ for $r = \infty$ requires
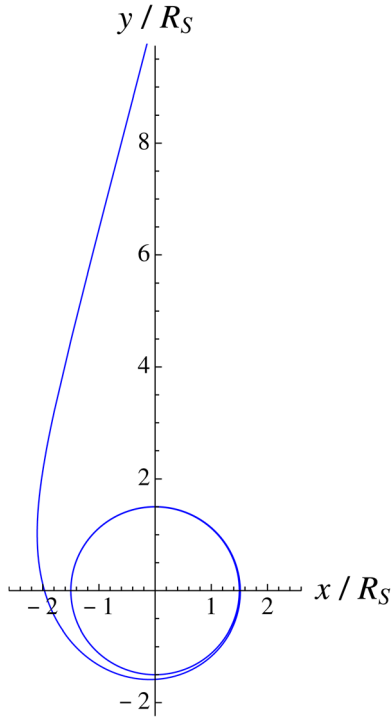
Fig. 2. An incoming trajectory with $b = b_{crit}$. The photon starts at infinity and spirals inward into a circular orbit at $r = 3R_S/2$.

$\alpha = \ln[(\sqrt{3} - 1)/(\sqrt{3} + 1)] \approx -1.317$. As ϕ increases the hyperbolic tangent approaches 1 and the photon approaches $r = 3R_S/2$ as $\phi \to \infty$. This trajectory, which corresponds to the horizontal line labeled $b = b_{crit}$ in Fig. 1, is shown in Fig. 2. Out-spiraling trajectories are obtained when $\phi_0 < \alpha$, provided $r > 3R_S/2$; they reach infinity for $\phi \to \alpha - \ln[(\sqrt{3} + 1)/(\sqrt{3} - 1)]$. Equation (24), on the other hand, was not included in Fig. 1 to avoid confusion. Given an initial starting point in its region of validity and an initial angle $\phi_0 > \alpha$, this solution gives an out-spiraling photon that ends at $r = 3R_S/2$ as $\phi \to \infty$. An example of such an orbit starting just outside the event horizon is provided in Fig. 3. If $\phi_0 < \alpha$ with α a large positive number, we get an in-spiraling solution that starts out near $r = 3R_S/2$ and reaches $r = R_S$ as $\phi \to \alpha - 2\ln[(\sqrt{3} + 1)/(\sqrt{3} - 1)]$.
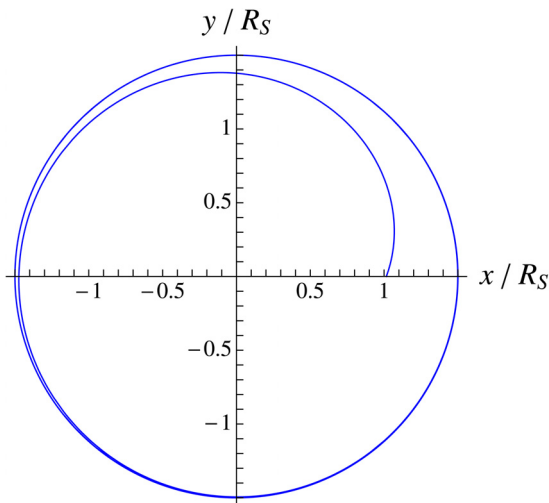
Fig. 3. An outgoing trajectory with $b = b_{crit}$. The photon starts near $r = R_S$ and spirals outward into a circular orbit at $r = 3R_S/2$.

B. $x > 1$ ($b < b_{crit}$; $L < L_{crit}$)

In this case, from Eq. (14) we see that ξ is again real, but now $0 < \xi < 1$. Equation (16) tells us that the first root is also real, with $-\infty < u_1 < -1/3$, while the other roots are complex conjugates:

$$u_2 = \frac{1}{6}\left[2 + \xi^{-2/3} + \xi^{2/3} + i\sqrt{3}\left(\xi^{-2/3} - \xi^{2/3}\right)\right] = u_3^*. \quad (25)$$

The orbit equation (12) can therefore be written as

$$\begin{aligned} u'^2 = f(u) &= (u - u_1)(u - u_2)(u - u_2^*) \\ &= (u - u_1)\left[(u - \operatorname{Re} u_2)^2 + (\operatorname{Im} u_2)^2\right]. \end{aligned} \quad (26)$$

We conclude that no turning points exist when $x > 1$, since $f(u)$ will never vanish for physical values of u. Indeed, the last form on the right-hand side of Eq. (26) shows that $f(u) > 0$ for negative u_1 and $0 < u < 1$, so all values of r are allowed: $R_S < r < \infty$. Thus, when $b < b_{crit}$, a photon emitted toward the central mass will inevitably fall into the black hole, whereas a photon emitted in the opposite direction will end up at infinity. The qualitative agreement with the top horizontal line in Fig. 1 is already apparent.

Equation (26) can now be transformed by standard methods into a canonical form. Following Lawden,[17] we make the substitution

$$w = \frac{u - q}{u + p} \quad (27)$$

with

$$p = \sqrt{\frac{1}{3}\left(\xi^{-4/3} + \xi^{4/3} + 1\right)} + \frac{1}{3}\left(\xi^{-2/3} + \xi^{2/3} - 1\right), \quad (28)$$

$$q = \sqrt{\frac{1}{3}\left(\xi^{-4/3} + \xi^{4/3} + 1\right)} - \frac{1}{3}\left(\xi^{-2/3} + \xi^{2/3} - 1\right). \quad (29)$$

Note that $p > 4/3$, $q > 2/3$, and $p > q$. Substitution into Eq. (26) leads, after some algebra, to

$$w'^2 = \frac{1}{2}(p + q)(1 - w^2)(\bar{k}^2 + k^2 w^2), \quad (30)$$

where

$$k = \sqrt{\frac{p + \operatorname{Re} u_2}{p + q}} = \frac{1}{\sqrt{2}}\left(1 + \frac{\sqrt{3}}{2}\frac{\xi^{-2/3} + \xi^{2/3}}{\sqrt{\xi^{-4/3} + \xi^{4/3} + 1}}\right)^{1/2} \quad (31)$$

and $\bar{k}^2 = 1 - k^2$. The range $0 < \xi < 1$ means that k is restricted to the range $(\sqrt{2 + \sqrt{3}})/2 < k < 1$. A final substitution

$$\psi = \sqrt{\frac{1}{2}(p + q)}\,\phi = \left[\frac{1}{3}\left(\xi^{-4/3} + \xi^{4/3} + 1\right)\right]^{1/4}\phi \quad (32)$$

yields the standard form[17,21,22]

$$\frac{dw}{d\psi} = \pm\sqrt{(1-w^2)(\bar{k}^2 + k^2 w^2)}, \tag{33}$$

and implies that our solution is

$$w = \mp \mathrm{cn}(\psi, k) + \text{constant}, \tag{34}$$

where $\mathrm{cn}(\psi, k)$ is the cn Jacobi elliptic function of modulus k. The constant can be absorbed into the definition of the initial angle, so that, solving for r from Eq. (27) we obtain the two alternatives

$$r = R_S \frac{1 \pm \mathrm{cn}(\psi, k)}{q \mp p\,\mathrm{cn}(\psi, k)}. \tag{35}$$

As pointed out above, for $x > 1$ our solutions should include photon trajectories that could begin or end at infinity. That Eq. (35) does allow for these possibilities is established by recalling that $p > q$ [see Eqs. (28) and (29)]. Hence, real solutions to $\mathrm{cn}(\psi, k) = \pm q/p$ exist and $r \to \infty$ for angles satisfying either condition. The meaning of the signs is easiest to understand if we go back to the relationship (27) between w and u and compute the derivative with respect to ϕ:

$$\frac{dw}{d\phi} = \frac{p+q}{(u+p)^2}\frac{du}{d\phi}. \tag{36}$$

For incoming (outgoing) photons, $du/d\phi > 0$ ($du/d\phi < 0$). Since both p and q are positive, identical inequalities hold for $dw/d\phi$. A glance at Eq. (33) then tells us that the upper signs in Eq. (35) describe incoming photons, whereas the lower signs apply for outgoing photons.

Large values of x are rather uninteresting because they imply small impact parameters, and a plot of Eq. (35) simply verifies the intuitive expectation that an incoming photon will follow an almost straight-line trajectory into the black hole. As a more compelling example, consider a photon starting out at infinity and aimed toward the central mass in such a way that the impact parameter differs only slightly from the critical value, say, $b_{\mathrm{crit}} - b = 10^{-5} b_{\mathrm{crit}}$ so that $x \approx 1 + 10^{-5}$. This choice will also serve as a comparison case to the trajectory in Fig. 2. From Eq. (14), $\xi \approx 0.99554$, and the remaining parameters needed in the solution

$$r = R_S \frac{1 + \mathrm{cn}(\psi, k)}{q - p\,\mathrm{cn}(\psi, k)} \tag{37}$$

can be computed from the formulas above with the results $\psi \approx (1 + 2.96 \times 10^{-6})\phi$, $p \approx 1.333342$, $q \approx 0.666669$, and $k \approx 0.9999996$. Dropping the constant in Eq. (34) leads to the convention that the initial angle (at $r = \infty$) is $\phi_0 \approx 1.316\,\mathrm{rad}$. From Eq. (37), the angle at the point where the photon crosses the event horizon at $r = R_S$ is $\phi_f \approx 14.254\,\mathrm{rad}$, and we conclude that the photon makes slightly over two full turns (relative to the line defined by the incoming direction) before falling into the black hole. This trajectory is shown in Fig. 4, which suggests that for impact parameters close to b_{crit} the photon tends to circle around $r = 3R_S/2$ before crossing the event horizon. The reader can verify that this is indeed the case, either by numerical calculations with x decreasing toward 1, or analytically by taking the limit of Eq. (37) as $b \to b_{\mathrm{crit}}$ ($x \to 1$) and using the
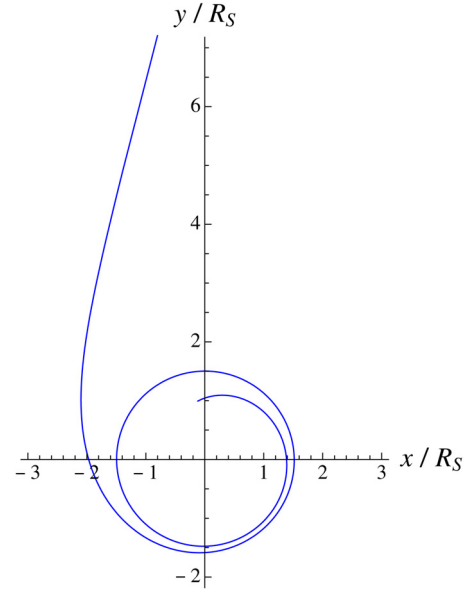
Fig. 4. An incoming trajectory with $b = (1 - 10^{-5})b_{\mathrm{crit}}$. The photon starts at infinity and crosses the event horizon after approximately two turns.

property that $\mathrm{cn}(\psi, 1) = \mathrm{sech}\,\psi$ to prove that Eq. (37) reduces to Eq. (23). The lower signs in Eq. (35) are illustrated in Fig. 5, which shows an outgoing photon emitted from a point near the event horizon, $r = 1.001 R_S$, with $x = 1.000037$. The limit as $b \to b_{\mathrm{crit}}$ will in this case take us back to Eq. (24).

C. $0 < x < 1$ ($b_{\mathrm{crit}} < b < \infty$; $L_{\mathrm{crit}} < L < \infty$)

In this case, Eq. (14) now yields a complex ξ, and the analysis of the roots, Eqs. (16)–(18), is somewhat simplified if we put

$$x = \cos\eta, \tag{38}$$
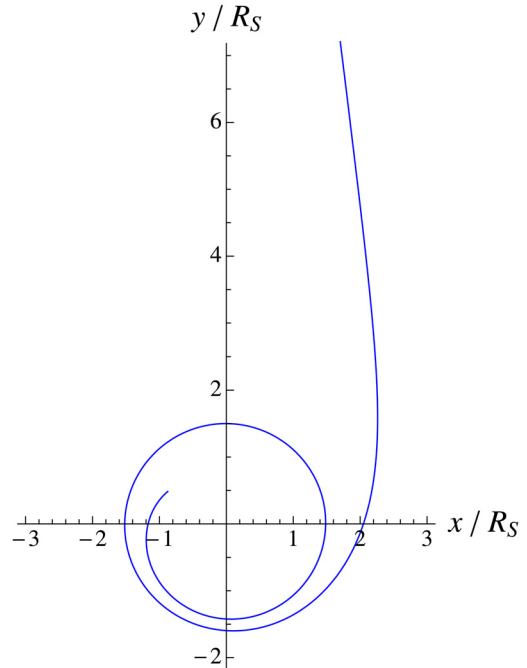
Fig. 5. An outgoing trajectory with $b < b_{\mathrm{crit}}$. The photon starts at $r = 1.001 R_S$ with $x = 1.000037$ and eventually reaches infinity.

with $0 < \eta < \pi/2$ in order to satisfy the bounds $0 < x < 1$. Given the impact parameter, η can be readily calculated from $\eta = \cos^{-1}(3\sqrt{3}R_S/2b)$. In terms of η, Eq. (14) becomes

$$\xi = e^{-i\eta}, \tag{39}$$

and all the roots are real numbers:

$$u_1 = -\frac{1}{3}\left[2\cos\left(\frac{2\eta}{3}\right) - 1\right], \tag{40}$$

$$u_2 = \frac{1}{3}\left[2\cos\left(\frac{2\eta + \pi}{3}\right) + 1\right], \tag{41}$$

$$u_3 = \frac{1}{3}\left[2\cos\left(\frac{2\eta - \pi}{3}\right) + 1\right]. \tag{42}$$

In this form, it is easy to see that the bounds on η imply the following bounds on the roots:

$$-\frac{1}{3} < u_1 < 0 < u_2 < \frac{2}{3} < u_3 < 1, \tag{43}$$

for any value of η.

We can now go back to the orbit equation (12). Since the function $f(u)$ on the right-hand side must be non-negative and u_1 is negative, we need the product $(u - u_2)(u - u_3)$ to be non-negative; hence the bounds (43) on the roots allow two regions of motion for the photons: either $u \geq u_3$, or $0 < u \leq u_2$. In other words, either $r \leq R_S/u_3$ or $R_S/u_2 \leq r < \infty$. The former corresponds to trajectories of the type illustrated by the short horizontal line to the left of the effective potential in Fig. 1, whereas the latter gives rise to trajectories of the type indicated by the line labeled $b > b_{\text{crit}}$. Note that $r = R_S/u_3$ and $r = R_S/u_2$ are turning points for these trajectories, since $f(u) = 0$ for $u = u_3$ and $u = u_2$.

Explicit formulas for these trajectories can be found as in the previous section by reducing the orbit equation to a canonical form. We begin with the case $r \leq R_S/u_3$. Guided by the standard integral form of some of the elliptic functions [see Eq. (47)], we use the fact that in the present case $u \geq u_3$ to introduce a sine squared by means of the substitution

$$u - u_1 = \frac{u_3 - u_1}{\sin^2 \chi}. \tag{44}$$

Equation (12) becomes

$$\chi'^2 = \frac{1}{4}(u_3 - u_1)(1 - k^2 \sin^2 \chi), \tag{45}$$

with

$$k = \sqrt{\frac{u_2 - u_1}{u_3 - u_1}}. \tag{46}$$

Legendre's form for the inverse sn function,[17]

$$\text{sn}^{-1}(\sin \chi, k) = \int_0^\chi \frac{d\varphi}{\sqrt{1 - k^2 \sin^2 \varphi}}, \tag{47}$$

makes it clear that the solution to Eq. (45), when written in terms of the angle

$$\psi = \frac{1}{2}\sqrt{u_3 - u_1}\,\phi, \tag{48}$$

is

$$\sin \chi = \pm \,\text{sn}(\psi - \alpha, k), \tag{49}$$

where α is a constant of integration. Substituting this expression into Eq. (44) yields the solution

$$\frac{R_S}{r} = u_1 + \frac{u_3 - u_1}{\text{sn}^2(\psi - \alpha, k)}. \tag{50}$$

As a concrete example, Fig. 6 shows an outgoing photon starting out at $r = 1.0053R_S$ with $b = 1.0002\,b_{\text{crit}}$ ($x \approx 0.9998$, $\eta \approx 0.0200$). The photon reaches a turning point at $r = R_S/u_3 \approx 1.4829\,R_S$ and falls inward across the event horizon after approximately 1.5 turns. This type of trajectory is very interesting because it implies that there are photons that cannot escape to infinity despite the fact that they were emitted *outside* the event horizon. The existence of such trajectories is, of course, already evident from Fig. 1, but only Eq. (50) can provide the quantitative details of the motion.

Our last case is $R_S/u_2 \leq r < \infty$. Instead of the substitution (44), the integral form (47) and the present condition $0 < u \leq u_2$ suggest that we should introduce a sine squared by means of the alternative

$$u - u_1 = (u_2 - u_1)\sin^2 \chi. \tag{51}$$

Following the same steps as above, we get

$$\frac{R_S}{r} = u_1 + (u_2 - u_1)\,\text{sn}^2(\psi - \alpha, k), \tag{52}$$

where the modulus k and the angle ψ are once again given by Eqs. (46) and (48), respectively. This solution encompasses the well-known approximate deflection calculations in the standard textbooks (see Sec. V), in addition to some less familiar behavior that is on display in the following figures. Figure 7 shows a photon that comes in from infinity with $x = 0.9955$ ($b = 1.0045\,b_{\text{crit}}$), loops around the central mass once, and then leaves toward infinity in a
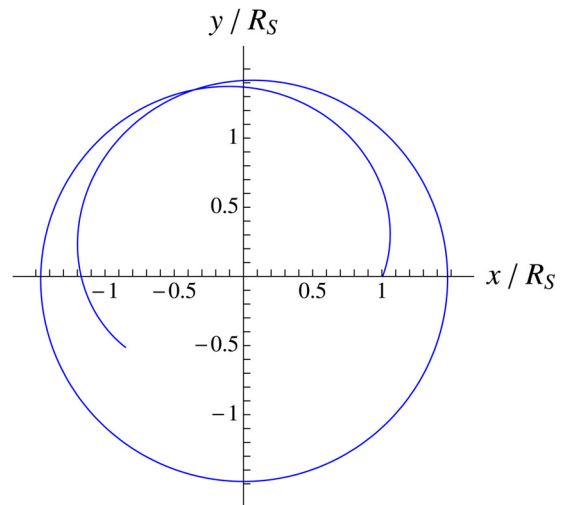
Fig. 6. A photon with $b > b_{\text{crit}}$ starts out at $r = 1.0053R_S$ with $x = 0.9998$, bounces off the effective potential, and falls into the black hole.
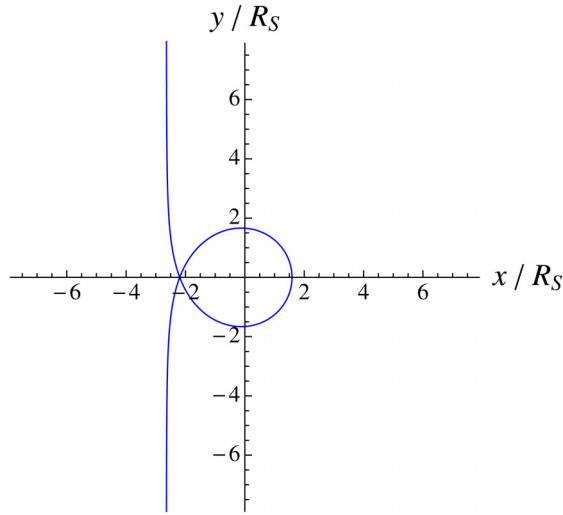
Fig. 7. A photon with $b > b_{\text{crit}}$ starting out at infinity with $x = 0.9955$.

direction that is essentially the same as that of the incoming trajectory. A simple measurement of the deflection angle in the geometrical-optics approximation would therefore be unable to distinguish this trajectory from one that experiences no deflection whatsoever, and one would have to resort to a measurement of, e.g., time delay effects to detect the presence of the central mass. Figure 8 is similar to the previous figure, except for the impact parameter; here $x = 0.9998$ ($b = 1.0002\, b_{\text{crit}}$) and we see that the photon makes an additional half turn and heads back toward the point of emission. Our final example, Fig. 9, depicts a photon with $x = 0.9999966$ ($b = 1.0000034\, b_{\text{crit}}$). Even though this photon loops more than twice around the black hole, to a far-away observer the net deflection would appear—provided the impact parameter is adjusted appropriately—indistinguishable from the value given by the small-angle approximation. From the knowledge that the turning points are at $r = R_S/u_2$, the reader can verify that in these three examples the (coordinate) distance of closest approach is very nearly $r = 1.5 R_S$. No incoming photon can get closer to the event horizon without falling into the black hole.
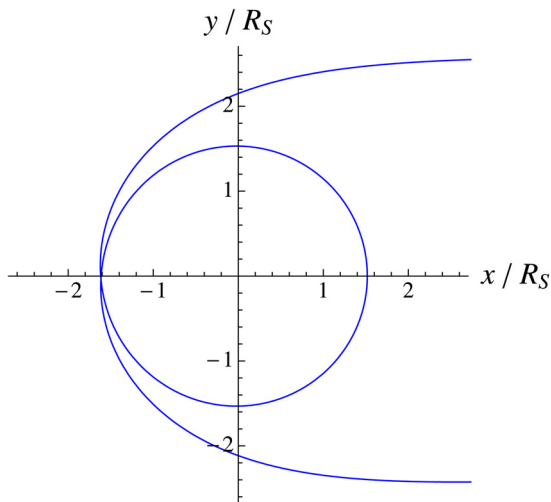
Fig. 8. A photon with $b > b_{\text{crit}}$ starting out at infinity with $x = 0.9998$.
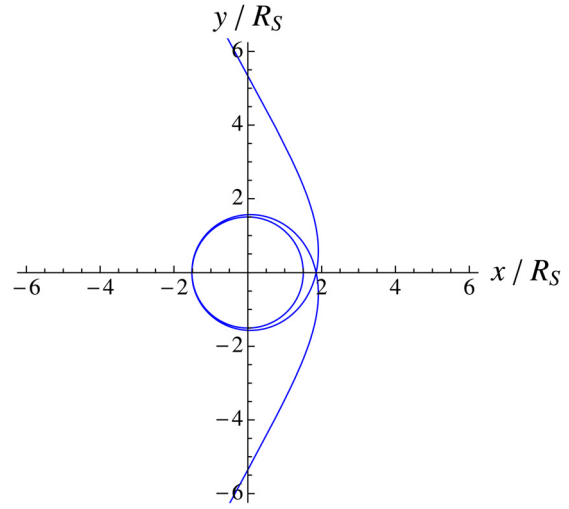
Fig. 9. A photon with $b > b_{\text{crit}}$ starting out at infinity with $x = 0.9999966$.

V. THE DEFLECTION ANGLE

We have seen in Sec. III that, in agreement with Fig. 1, there is only one class of trajectories that will allow photons coming in from asymptotic infinity to approach the central mass, and then escape to infinity again. These trajectories are given by Eq. (52), and it is our purpose in this section to develop exact formulas for the deflection angles based on that solution.

To this end, it will prove convenient to choose the integration constant α so that $\phi = 0$ at periapsis, when $r = R_S/u_2$. Because for real arguments the Jacobi elliptic function $\mathrm{sn}(z, k)$ goes from zero at $z = 0$ to a maximum of 1 at $z = K$, where K is the complete elliptic integral of the first kind

$$K(k) = \int_0^{\pi/2} \frac{d\varphi}{\sqrt{1 - k^2 \sin^2 \varphi}},\tag{53}$$

and then back to zero at $z = 2K$ in a periodic fashion (the elliptic functions are actually doubly periodic for complex arguments), our convention can be incorporated by setting $\alpha = -K$ in Eq. (52). The solution now reads

$$\frac{R_S}{r} = u_1 + (u_2 - u_1)\, \mathrm{sn}^2(\psi + K, k).\tag{54}$$

From the symmetry of the motion about $\phi = 0$ it should be clear that, if $\phi_{-\infty}$ denotes the angle as the photon starts at infinity on its way in and ϕ_{∞} the angle as the photon reaches infinity on its way out, then $\phi_{-\infty} = -\phi_{\infty}$ and the net change in the angle must be $\Delta\phi = 2\phi_{\infty} = 2|\phi_{-\infty}|$. Equation (54) implies that $r = \infty$ will be reached when

$$\psi_{\pm\infty} + K = \mathrm{sn}^{-1}\sqrt{\frac{-u_1}{u_2 - u_1}}.\tag{55}$$

The inverse sn function is multivalued, but our convention for ϕ restricts the solutions of Eq. (55) to the interval $(0, 2K)$. It follows that the solution for $\phi_{-\infty}$ must be sought in the first quarter-period $(0, K)$, whereas ϕ_{∞} will be obtained if we adopt the solution in the second quarter-period $(K, 2K)$. Recalling the definition (48) of ψ and using Eq. (55) to solve for $\phi_{-\infty}$, we arrive at the exact formula for the angular change

$$\Delta\phi = \frac{4}{\sqrt{u_3 - u_1}} \left(K - \text{sn}^{-1} \sqrt{\frac{-u_1}{u_2 - u_1}} \right). \quad (56)$$

We have chosen to work with sn^{-1} in the interval $(0, K)$ for a very simple practical reason: most of the expansions found in the published literature as well as in software packages for sn and sn^{-1} are given in the first quarter-period. This will prove helpful next when we try to check our formula against the well-known result for the deflection of light in the weak-field limit.

In order to proceed in this direction we require approximations of all the quantities involved. The weak-field limit is applicable when the photon remains at large distances from the central mass at all times, i.e. when $r_{\min} = R_S/u_2 \gg R_S$, or $u_2 \ll 1$. Equations (38) and (41) then reveal that $\eta \approx \pi/2$ and $x \ll 1$ are equivalent statements. There are therefore three alternatives for the expansion of $\Delta\phi$; we shall opt for an expansion in powers of x because the impact parameter is directly measurable in the flat spacetime at asymptotic infinity. An expansion in powers of u_2, on the other hand, would involve the determination of a coordinate distance in the curved spacetime near the central mass.

For small x we have

$$u_1 = -\frac{2x}{3\sqrt{3}} + \frac{2x^2}{27} - \frac{5x^3}{81\sqrt{3}} + O(x^4), \quad (57)$$

$$u_2 = \frac{2x}{3\sqrt{3}} + \frac{2x^2}{27} + \frac{5x^3}{81\sqrt{3}} + O(x^4), \quad (58)$$

$$u_3 = 1 - \frac{4x^2}{27} + O(x^4). \quad (59)$$

Terms up to third order must be kept in the expansion of the roots if we wish to find the lowest-order correction to the well-known result $\delta\phi = 2R_S/b$ for the deflection angle. The modulus k and the argument of the sn^{-1} in Eq. (56) are

$$k^2 = \frac{4x}{3\sqrt{3}} - \frac{8x^2}{27} + \frac{50x^3}{81\sqrt{3}} + O(x^4), \quad (60)$$

$$\sqrt{\frac{-u_1}{u_2 - u_1}} = \frac{1}{\sqrt{2}} - \frac{x}{6\sqrt{6}} - \frac{x^2}{216\sqrt{2}} - \frac{5x^3}{144\sqrt{6}} + O(x^4). \quad (61)$$

The small-k expansions of $K(k)$ and $\text{sn}^{-1}(z, k)$ can be found in the literature,[17] or developed directly from Eqs. (47) and (53):

$$K(k) = \frac{\pi}{2} + \frac{\pi}{8} k^2 + \frac{9\pi}{128} k^4 + \frac{25\pi}{512} k^6 + O(k^8), \quad (62)$$

$$\text{sn}^{-1}(z, k) = \sin^{-1}(z) + \frac{1}{4} k^2 \left[\sin^{-1}(z) - z\sqrt{1 - z^2} \right]$$
$$+ \frac{3}{64} k^4 \left[3\sin^{-1}(z) - (3z + 2z^3)\sqrt{1 - z^2} \right]$$
$$+ \frac{5}{768} k^6 \left[15\sin^{-1}(z) - (15z + 10z^3 + 8z^5) \right.$$
$$\left. \times \sqrt{1 - z^2} \right] + O(k^8). \quad (63)$$

Combining Eqs. (57)–(63) and substituting into Eq. (56) yields

$$\Delta\phi = \pi + \frac{4}{3\sqrt{3}} x + \frac{5\pi}{36} x^2 + \frac{128}{243\sqrt{3}} x^3 + O(x^4). \quad (64)$$

The deflection relative to the straight-line motion that light would follow in empty space is $\delta\phi = \Delta\phi - \pi$. Recalling that $x = 3\sqrt{3}R_S/2b$, we get

$$\delta\phi \approx 2 \frac{R_S}{b} + \frac{15\pi}{16} \left(\frac{R_S}{b} \right)^2 + \frac{16}{3} \left(\frac{R_S}{b} \right)^3, \quad (65)$$

and the first term on the right-hand side confirms that Eq. (56) reproduces the standard first-order deflection. The second term agrees with the approximate calculation of Epstein and Shapiro[23] within the framework of the PPN formalism (see also Ref. 24). It is very small under solar-system conditions, amounting to just $10\,\mu$as for light grazing the Sun. While this is beyond the accuracy of current observations (about 1 mas for the ESA's Hipparcos space astrometry mission), the ESA's Gaia mission, launched in December 2013, is expected to reach an accuracy of about $24\,\mu$as.[25] The third term is roughly 11 orders of magnitude smaller than the first term.

A strong-field approximation can also be derived from Eq. (56). We leave it to the reader to show that, for $x \to 1$,

$$\Delta\phi \approx \ln \left[\frac{432 (2 - \sqrt{3})^2}{1 - (3\sqrt{3}R_S/2b)^2} \right]. \quad (66)$$

Figure 10 shows the monotonic behavior of the deflection $\delta\phi$ obtained from Eq. (56) as a function of the impact parameter. As $b \to b_{\text{crit}} = 3\sqrt{3}R_S/2$, $\delta\phi$ increases without bound, indicating a photon that tends to settle into a circular orbit at $r = 1.5R_S$. The solar-system result of $1.75''$ is not visible in this diagram because $b/R_S \approx 2.4 \times 10^5$ for light grazing the Sun.

Photons completing one or more turns must have impact parameters $b \to b_{\text{crit}}$. The condition $\Delta\phi = n\pi$, with $n \geq 2$,
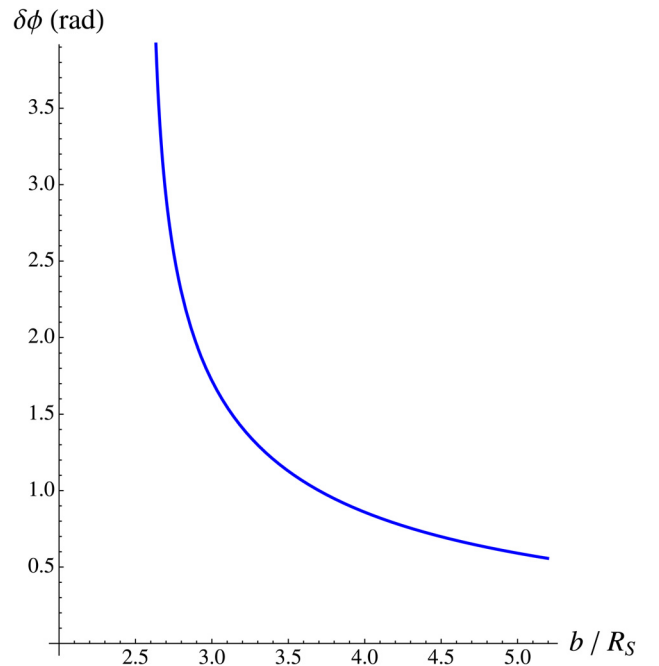
Fig. 10. The deflection $\delta\phi$ (in radians) implied by Eq. (56) as a function of the impact parameter b (in units of the Schwarzschild radius).

allows us to identify photons that continue (seemingly unde-flected) along the original direction of motion after one full turn ($n = 3$), two full turns ($n = 5$), and so on; Fig. 7 shows $n \approx 3$. For n even, the same condition singles out photons that must return to the source without an additional turn ($n = 2$), with one additional turn ($n = 4$), and so on; Fig. 8 shows $n \approx 4$. The appropriate impact parameters are, from Eq. (66),

$$b_n \approx \frac{3\sqrt{3}R_S}{2\sqrt{1 - 432\,(2 - \sqrt{3})^2\,e^{-n\pi}}}. \tag{67}$$

For half-integer n the photons exit at right angles to the origi-nal direction of motion.

From a practical point of view, it is important to notice that the exact formula (56) for $\Delta\phi$ implies that a measure-ment of the angular change can be used to infer the ratio R_S/b only. This is apparent in the approximations (65) and (66). In the general case, it follows from the observation that Eq. (56) is a function of the roots, Eqs. (40)–(42), of $f(u) = 0$, which are, in turn, completely determined by $\eta = \cos^{-1}(3\sqrt{3}R_S/2b)$. Therefore, the elucidation of quanti-ties such as the impact parameter b, the distance of closest approach $r_{\min} = R_S/u_2$, or the mass of the black hole require additional experimental input. As we show next, this infor-mation can be obtained by measuring the time delay differ-ence between light rays.

Since this is most likely to be the case in practice, let us assume that the source and the detector are very far away from the black hole. From Eqs. (7), (8), and (12),

$$dx^0 = \pm \frac{R_S^2}{b} \frac{du}{u^2(1 - u)\sqrt{f(u)}} \tag{68}$$

and the total time delay Δx^0 is twice the delay from the source to periapsis

$$\Delta x^0 = 2\frac{R_S^2}{b}\int_0^{u_2} \frac{du}{u^2(1 - u)\sqrt{f(u)}}. \tag{69}$$

While it is possible to write down an expression for Δx^0 in terms of elliptic functions, the answer is very cumbersome and, fortunately, unnecessary for our purposes. An experi-mentally more useful quantity is the rate of change $\partial\Delta x^0/\partial b$, since two light rays that are known to originate simultane-ously at the source can only differ in their time delays and deflection angles if they have different impact parameters. A fairly straightforward computation using Eqs. (41) and (69) and $\eta = \cos^{-1}(3\sqrt{3}R_S/2b)$ shows that

$$\frac{\partial\Delta x^0}{\partial b} = b\frac{\partial\Delta\phi}{\partial b}, \tag{70}$$

with

$$\Delta\phi = 2\int_0^{\phi(r_{\min})} d\phi = 2\int_0^{u_2} \frac{du}{\sqrt{f(u)}} \tag{71}$$

the angular change of Eq. (56). Thus, if we can independ-ently ascertain that two light rays deflected by a single black hole were produced simultaneously at the source, Eq. (70) tells us that the impact parameter b can be found by

computing the ratio of the observed difference in their time delays to the difference in angular changes. A plot of $\delta\phi$ against b can then be constructed and the black hole mass determined by a best fit of the angular deflection data to the exact prediction of Eq. (56) (see Fig. 10).

As a check of Eq. (70), consider the approximation of Eq. (64) for large impact parameters. Our formula yields

$$\frac{\partial\Delta x^0}{\partial b} \approx -2\frac{R_S}{b} - \frac{15\pi}{8}\left(\frac{R_S}{b}\right)^2 - 16\left(\frac{R_S}{b}\right)^3, \tag{72}$$

and the first term is easily verified to be in agreement with the Shapiro time delay.

A small impact parameter ($b \to b_{\mathrm{crit}}$) approximation fol-lows from Eq. (66); we find the simple result

$$\frac{\partial\Delta x^0}{\partial b} \approx -3\sqrt{3}\frac{R_S}{\delta b}, \tag{73}$$

with $\delta b \equiv b - b_{\mathrm{crit}}$ such that $\delta b/b_{\mathrm{crit}} \ll 1$.

VI. CONCLUSION

In this article, we have developed a complete classification of the orbits of massless particles around a Schwarzschild black hole. These exact solutions led, in turn, to an exact formula for the deflection angle. When expanded in a power series in R_S/b, our formula not only reproduces the known first- and second-order terms but also allows for a fairly sim-ple computation of higher-order corrections. When com-bined with a similar exact expression for the time delay, the deflection angle formula leads to a new method for the deter-mination of black hole masses that does not rely on the pres-ence of a companion. A related but different method has been proposed by Müller.[7]

As pointed out in the Introduction, a classification of the orbits of massless particles was given by Chandrasekhar almost exactly thirty years ago. A brief summary of the dif-ferences between his approach and the one presented in this paper might be helpful to the reader.

(i) Chandrasekhar uses a mathematical classification of the orbits, that is, a classification based entirely on the roots of a cubic in $1/r$. In this paper, we approached the problem from the point of view of the impact pa-rameter, a familiar physical quantity that is directly accessible in observational astronomy.

(ii) Chandrasekhar's solutions are given in parametric form $(r(\chi), \phi(\chi))$, which is convenient for some applications. However, since χ appears in the argu-ment of the incomplete elliptic integral of the first kind, inverting to obtain $r(\phi)$ is not trivial (see, e.g., Cadez and Kostic[6]). The solutions in this paper directly give $r(\phi)$ in terms of Jacobi elliptic functions without going through an intermediate parametric form.

(iii) Chandrasekhar's solutions are also functions of the coordinate perihelion distance, a quantity that cannot be measured directly. Our solutions provide a practi-cal way to compute the perihelion distance using as input the measurable impact parameter.

(iv) Chandrasekhar gives four plots that help visualize the behavior of the solutions. Unfortunately, his three most interesting figures are labeled either by the

coordinate perihelion distance, or by an imaginary eccentricity. We hope that Figs. 2–9 in this paper, which are based on the initial position and impact parameter of the photon, will provide additional insights into the qualitative behavior of the trajectories.

[a] Electronic mail: gerardom@csufresno.edu

[1] J. Droste, "The Field of a Single Centre in Einstein's Theory of Gravitation, and the Motion of a Particle in that Field," Koninklijke Nederlandsche Akademie van Wetenshappen Proceedings **19**, 197–1563 (1917). Reprinted in Gen. Rel. Grav. **34**, 1545–1563 (2002).

[2] Y. Hagihara, "Theory of the Relativistic Trajectories in a Gravitational Field of Schwarzschild," Jpn. J. Astron. Geophys. **8**, 67–176 (1931). Available on the Smithsonian/NASA Astrophysics Data System, <http://articles.adsabs.harvard.edu/full/1930JaJAG…8…67H/>.

[3] B. Mielnik and J. Plebański, "A study of geodesic motion in the field of Schwarzschild's solution," Acta Phys. Polon. **21**, 239–268 (1962).

[4] C. Darwin, "The gravity field of a particle," Proc. Roy. Soc. A **249**, 180–194 (1959).

[5] S. Chandrasekhar, *The Mathematical Theory of Black Holes* (Clarendon Press, Oxford, 1983).

[6] A. Čadež and U. Kostić, "Optics in the Schwarzschild spacetime," Phys. Rev. D **72**, 104024-1–10 (2005).

[7] T. Müller, "Einstein rings as a tool for estimating distances and the mass of a Schwarzschild black hole," Phys. Rev. D **77**, 124042-1–11 (2008).

[8] G. Gibbons and M. Vyska, "The application of Weierstrass elliptic functions to Schwarzschild null geodesics," Class. Quant. Grav. **29**, 065016 (2012), e-print arXiv:1110.6508v2 \gr-qc].

[9] E. Hackmann and C. Lämmerzahl, "Geodesic equation in Schwarzschild-(anti-)de Sitter space-times: Analytical solutions and applications," Phys. Rev. D **78**, 024035-1–22 (2008).

[10] E. Hackmann, B. Hartmann, C. Lämmerzahl, and P. Sirimachan, "Complete set of solutions of the geodesic equation in the space-time of a Schwarzschild black hole pierced by a cosmic string," Phys. Rev. D **81**, 064016-1–18 (2010).

[11] C. Møller, *The Theory of Relativity*, 2nd ed. (Clarendon Press, Oxford, 1972).

[12] B. F. Schutz, *A First Course in General Relativity*, 2nd ed. (Cambridge U.P., Cambridge, 2009).

[13] C. W. Misner, K. S. Thorne, and J. A. Wheeler, *Gravitation*, 2nd ed. (W. H. Freeman, New York, 1973).

[14] W. Rindler, *Relativity: Special, General, and Cosmological*, 2nd ed. (Oxford U. P., New York, 2006).

[15] S. Carroll, *Spacetime and Geometry: An Introduction to General Relativity* (Pearson Addison Wesley, San Francisco, 2004).

[16] H. Stephani, *Relativity: An Introduction to Special and General Relativity* (Cambridge U. P., Cambridge, 2004).

[17] D. F. Lawden, *Elliptic Functions and Applications*, Applied Mathematical Sciences v. 80 (Springer Verlag, New York, 1989). We follow Lawden's convention on the use of the modulus k throughout this paper; other references prefer the parameter $m = k^2$ instead.

[18] T. E. Baker and A. Bill, "Jacobi elliptic functions and the complete solution to the bead on the hoop problem," Am. J. Phys. **80**, 506–514 (2012).

[19] E. T. Whittaker, *A Treatise on the Analytical Dynamics of Particles and Rigid Bodies*, 4th ed. (Dover, New York, 1944).

[20] W. D. MacMillan, *Theoretical Mechanics: Statics and Dynamics of a Particle* (McGraw-Hill, New York, 1927).

[21] I. S. Gradshteyn and I. M. Ryzhik, *Table of Integrals, Series and Products*, 4th ed. (Academic Press, New York, 1980).

[22] M. Abramowitz and I. A. Stegun, *Handbook of Mathematical Functions* (U.S. Government Printing Office, Washington, 1972). Available electronically at <http://www.nr.com/aands/> or <http://people.math.sfu.ca/~cbm/aands/>. See also the NIST Digital Library of Mathematical Functions at <http://dlmf.nist.gov/>.

[23] R. Epstein and I. I. Shapiro, "Post-post-Newtonian deflection of light by the Sun," Phys. Rev. D **22**, 2947–2949 (1980).

[24] J. Bodenner and C. M. Will, "Deflection of light to second order: A tool for illustrating principles of general relativity," Am. J. Phys. **71**, 770–773 (2003).

[25] Gaia Web site, <http://sci.esa.int/gaia/>. Unfortunately, the SIMLite Astrometric Observatory, which was expected to reach an accuracy of a few microarcseconds, was canceled by NASA in December of 2010.

Duplex Geryk Mechanical Air Pump

From the 1909 catalogue of the Central Scientific Company of Chicago.: "This is an English pump (Fleuss' patents) and is strictly a mechanical device with no valves in the usual sense of the word; the pistons work in oil, which continuously follows and seals the inlets and outlets, so that leakage is impossible. There are no inside working parts to wear out, replace or adjust." The imported pump was duty free and cost $96.50. This example is at the University of Arkansas. (Notes and photograph by Thomas B. Greenslade, Jr., Kenyon College)